International Journal of Heat and Mass Transfer 51 (2008) 5655–5661

Contents lists available at ScienceDirect

International Journal of Heat and Mass Transfer

journal homepage: www.elsevier.com/locate/ijhmt

Numerical simulation of local temperature distortions during ice nucleation of cells in suspension

D. Kandra, R.V. Devireddy *

Bioengineering Laboratory, Department of Mechanical Engineering, Louisiana State University, Baton Rouge, LA, USA

ARTICLE INFO

Article history:
Received 2 November 2007
Received in revised form 4 April 2008
Available online 4 June 2008

Keywords:
Ice nucleation
Latent heat
Apparent heat capacity
Fourier heat conduction

ABSTRACT

Knowledge of intercellular ice formation in cells embedded in an extra-cellular suspension is essential for effective design of freezing protocols. The presence of cell membrane causes super-cooling of the intracellular region, which nucleates at much lower temperatures than the surrounding extra-cellular space and is accompanied by the exothermic release of the latent heat. This is a dynamic process and causes thermal distortions in and around the cell where nucleation occurs. In the present study, an attempt has been made to numerically determine the magnitude of thermal distortion (ΔT) and the time (dt) it takes for this distortion to damp out to the local temperature. A two-dimensional computational model is presented in which the maximum thermal distortions (with an assumed cell diameter of 50 μm, nucleating at −5 °C while being cooled at 5 °C/min; denoted as Scenario 1) and the lowest-possible thermal distortions (with an assumed cell diameter of 5 μm, nucleating at −20 °C while being cooled at 100 °C/min; denoted as Scenario 2) are determined. Extensive computations have been performed assuming either the presence of a single, dual, or four cells in suspension. It is expected that these representative results would serve the purpose of estimating an effective sampling rate of microscale thermocouples currently being fabricated and of other biomedical devices used to measure intracellular ice formation.

1. Introduction

The process of freezing biological tissue continues to be actively studied because of its central role in two important biomedical applications, cryopreservation and cryosurgery [1–7]. Cryopreservation (i.e., the process of freezing at controlled rates, storage in liquid nitrogen, and subsequent thawing) is a leading candidate for fulfilling the immediate and urgent need for storage, banking, and transport of native and artificial tissues prior to use. Cryosurgery is the use of low temperature to destroy malignant tissue *in vivo* (inside the body) using minimally invasive cryosurgical probes. Examples of cryosurgical methods include destruction of prostate cancer, uterine fibroids, and colo-rectal carcinoma. Examples of cryopreservation protocols include storage of mammalian sperm for gene banks and hepatocytes for use in bio-artificial liver devices and xenobiotic drug studies.

Numerical modeling has proven to be extremely useful in studying tissue freezing problems [8–14]. Most models of tissue thermal response assume the tissue to be a single-compartment homogeneous medium, e.g., pure water or isotonic saline. In this case, phase change is described by the phase diagram of the chosen medium. Mathematically, latent heat content is assumed to be a function of temperature $L(T)$, and the energy equation is solved in the enthalpy form or with a modified specific heat which incorporates this function [8–14]. From several experiments dating back to the late 18th century, it is known that the process of freezing in suspensions of cells and tissues is significantly different from freezing of inanimate materials [15–21]. In native biological tissues, a significant portion of the water in tissue is intracellular, separated from the surrounding tissue by a cell membrane. Basically, during tissue freezing there are three macroscopic domains: an unfrozen region, a partially frozen or mushy region, and a frozen region. The equations describing the heat transfer in the unfrozen and frozen region can be any of the versions of the standard bioheat equation reported extensively in the literature [8–14]. The process of freezing occurs in the partially frozen or the mushy region and is characterized by the presence of the extra-cellular dendritic ice crystals in thermodynamic equilibrium with the extracellular solution and by dehydrating unfrozen cells or by nucleating frozen cells. Phase change in tissue is, therefore, governed not only by the phase diagram for tissue fluids but also by the dynamics of the biophysical processes of cellular dehydration and intracellular ice formation (IIF).

We have recently presented a coupled tissue freezing model [22] in which the coupling of the biophysical phenomena (water transport and IIF) into the calculation of phase change is accomplished by creating a latent heat function similar to those used in

* Corresponding author. Tel.: +1 225 578 5891; fax: +1 225 578 5924.
E-mail address: devireddy@me.lsu.edu (R.V. Devireddy).

0017-9310/$ - see front matter © 2008 Elsevier Ltd. All rights reserved.
doi:10.1016/j.ijheatmasstransfer.2008.04.026

Nomenclature

B	cooling rate (°C/min)
c	specific heat (kJ/kg K)
L	latent heat of fusion of the extracellular isoosmotic salt solution, is a function of temperature, T (kJ/kg)
k	thermal conductivity (kW/m K)
Q	heat input due to ice nucleation within a cell (kW/m^3)
R	radius of the nucleating cell (μm)
$T(x,y,t)$	temperature as a function of spatial location (x,y) and time, t (°C)
T_{ph}	melting or phase change temperature (°C)
T_{nuc}	temperature at which ice nucleates within the cell (°C)
ΔH_f	latent heat of fusion of the intracellular isoosmotic salt solution, is a function of ice nucleation temperature, T_{nuc} (kJ/kg)
ΔT	local temperature rise, relative to the temperature without ice nucleation (°C)
t	time (s)
dt	time required to dampen out the local thermal distortion (s)
V	volume of the nucleating cell (M^3)
x and y	spatial location (M)
ρ	density (kg/m^3)
Subscripts	
l	liquid unfrozen
s	solid frozen

enthalpy or modified specific heat formulations. That is, the latent heat is a function of both temperature and time, $L(T,t)$. The exact functional dependence of $L(T,t)$ is quite complex and is dependent not only upon the biophysical parameters governing the tissue system being frozen but also the cooling stress being imposed [22]. The numerical results from the coupled model were compared with the results from the more commonly used uncoupled model (enthalpy model) in two test cases (rat liver tissue and AT-1 tumor tissue) under two different cooling conditions (cryopreservation and cryosurgery). The results for both the coupled and uncoupled models were found to be very similar, thus suggesting that the microscale biophysical processes which occur in the biological tissue during freezing do little to limit the rate at which phase change can occur. This finding indicates that the uncoupled approach to numerical solution would be adequate to accurately determine thermal history for the tissue types studied. However, the microscopic phenomena, especially IIF (which is a highly localized phase change event) will still generate local thermal distortions around the nucleating cell. In the present study, an attempt has been made to numerically determine the magnitude of thermal distortion (ΔT) and the time (dt) it takes for this distortion to dampen out to the local temperature. We defined the magnitude of the thermal distortion (ΔT) as the relative difference in the temperature between the center of the cell that is nucleating and the *a priori* calculated temperature without ice nucleation. It is expected that this knowledge will be critical to further the development of a novel class of instruments based on micro-fabricated thermoelectric sensors (utilizing the Seebeck effect) and actuators (utilizing the Thompson effect).

2. Materials and methods

Based on earlier results by Devireddy et al. [22] that account for the effect of microscopic heat transfer phenomena on macroscale freezing response (thermal history, freeze front, etc.), we propose to use the Fourier heat conduction equation to simulate freezing of the cells in suspension and a point-wise heat input/source term to account for the intracellular ice nucleation phenomena as shown below:

$$\frac{\partial}{\partial x}\left(k_s(T)\frac{\partial T_s}{\partial x}\right)+\frac{\partial}{\partial y}\left(k_s(T)\frac{\partial T_s}{\partial y}\right)+Q=\rho_s c_s(T)\frac{\partial T_s}{\partial t} \quad (1)$$

$$\frac{\partial}{\partial x}\left(k_l\frac{\partial T_l}{\partial x}\right)+\frac{\partial}{\partial y}\left(k_l\frac{\partial T_l}{\partial y}\right)+Q=\rho_l c_l\frac{\partial T_l}{\partial t} \quad (2)$$

Eqs. (1) and (2) are the governing equations applicable for the frozen and unfrozen regions of the cell suspension, respectively. To accurately predict the thermal distortions the thermophysical properties are taken to be temperature dependent [[22]; Table 1]. Eqs. (1) and (2) are coupled using the apparent heat capacity method [8–14,22–24]. To represent a freezing process in a biological system as closely as possible, the extracellular solution is assumed to be freezing and releasing latent heat as a function of temperature, $L(T)$. Under these conditions the "effective" specific heat can be approximated as: $c_p = L(T)/\Delta T$, where $L(T)$ is the latent heat released at temperatures ranging between −20 °C and −0.53 °C and based on our previous experience, the smoothening function, ΔT was set to 0.01 °C. The functional form of the fraction of latent heat of fusion released by the extracellular solution at the solid–liquid freeze-front interface is given as [25]

$$L(T)=L^*\left[1-\frac{A}{T_{ph}-T+A}\right] \quad (3)$$

where T_{ph} is −0.53 °C, $T < T_{ph}$ and A is called the Avrami constant and is equal to 0.53. As can be seen the magnitude of heat released between −0.53 °C and −20 °C is $0.9735 \cdot L$ and is accordance with earlier experimental observations of heat release during freezing of salt solutions [9,10,25]. A more detailed description of the numerical model is presented elsewhere [9,10,22] and, in the interest of brevity, will not be repeated here. Note that $Q = \rho_l \cdot \Delta H_f(T_{nuc}) \cdot V$, and represents the instantaneous heat input from intracellular ice formation within a cell nucleating at T_{nuc}. The temperature at which this heat is released or the temperature for the formation of intracellular ice (T_{nuc}) is chosen *a priori* and, as described below, was either −5 °C or −20 °C. We further assumed that the embedded cell while nucleating represents a highly localized "point" heat source in the suspension being cooled at a constant and predetermined rate. We then determined the temperature distortions due to the release of latent heat during ice nucle-

Table 1
A listing of the thermal properties used in the numerical model

Thermophysical constant	Value and units
k	0.6 W/m-K (unfrozen) 2.24 + 0.005975(273-T)$^{1.156}$ W/m-K (Frozen)
c	4200 J/kg-K (unfrozen) 7.16T + 138 J/kg-K (frozen)
ρ	999 kg/m^3 (unfrozen) 921 kg/m^3 (frozen)
L	335 J/kg
T_{ph}	−0.53 °C
T_{nuc}	−5 °C or −20 °C
ΔH_f	320 J/kg (when T_{nuc} = −5 °C) or 290 J/kg (when T_{nuc} = −20 °C)

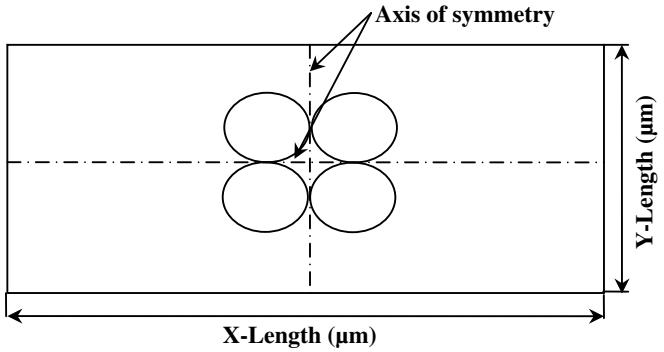

Fig. 1. Computational domain showing the four cells and the axis of symmetry.

ation using a custom-written Fortran code. To facilitate easy comparison between various computational scenario's we defined the magnitude of the temperature distortions (ΔT) as the difference in the temperature field within the computational space with and without ice nucleation in the cell. The computational domain is discretized using the finite control volume method with a spatial grid spacing of 0.001 μm and the overall computational space was 4 cm^2 [23,24,26]. All simulations were performed on a Dell desktop computer (see Table 1).

Figs. 1 and 2 show the geometry of the computational domain for four cells and two cells in suspension, respectively. Note that the assumption of symmetry results in the analysis of only one quadrant of Fig. 1 and one half separated by the axis of symmetry in Fig. 2. For the purposes of the analysis being performed in this study, the additional horizontal line of symmetry in Fig. 2 was not utilized. The boundary conditions at the line of symmetry are of second kind (adiabatic) and the surface temperatures are iteratively modified so that the cell center is always subjected to a constant, predetermined cooling rate. A two-dimensional computational model was used to study two specific conditions: Scenario 1: a cell with a diameter of 50 μm nucleating at −5 °C while being cooled at 5 °C/min and Scenario 2: a cell with a diameter of 5 μm nucleating at −20 °C while being cooled at 100 °C/min. For each scenario, we investigated the effect of having one, two, or four cells simultaneously nucleating within the computational domain. Thus, six different sets of numerical simulations were performed. The choice of the cell geometries, the cooling rates, and the temperature of ice nucleation were based on the fact that the pre-selected combinations in Scenario 1 and 2 would lead to a maximum and minimum thermal distortion around the nucleation zone in a realistic cellular system undergoing a freezing process [10–14,22].

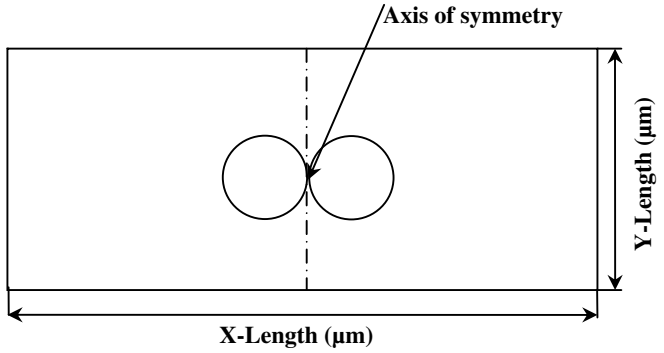

Fig. 2. Computational domain showing the two cells and the axis of symmetry.

3. Results

Our numerical model was compared with the standard analytical solution for the same geometry dimensions in the case of constant thermophysical properties [27,28]. The results differed from the analytical solution by ~0.1% (data not shown, in the interest of brevity) and validated our numerical model.

Fig. 3 (at dt = 0 s) and Fig. 4 (at dt = 1.96 s) show the computed thermal distortion contours caused due to the nucleation of four

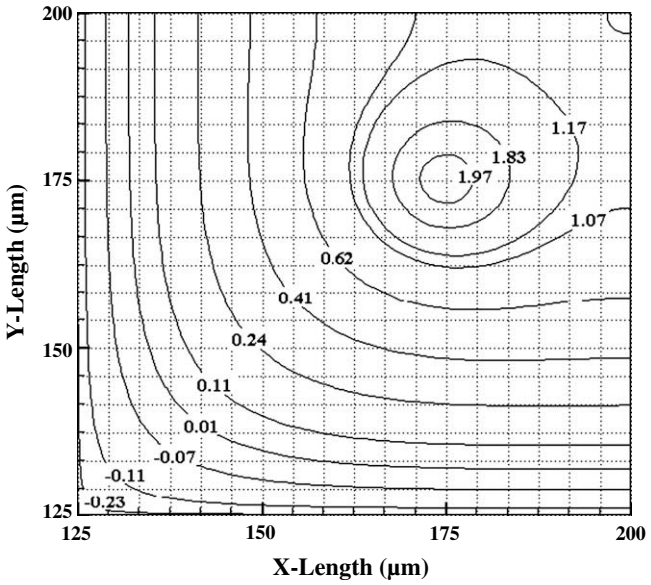

Fig. 3. Immediate (dt = 0) thermal distortions due to the simultaneous nucleation of ice within all the four cells, shown in Fig. 1. One of the nucleating cells is centered at (x,y) coordinates of (175,175). The nucleating cell is assumed to be 50 μm in diameter, being cooled at 5 °C/min and ice nucleates within all the cells at −5 °C. Note that at one of the cell centers (175,175) that ΔT = 1.97 °C. Various isotherms are also shown in the figure.

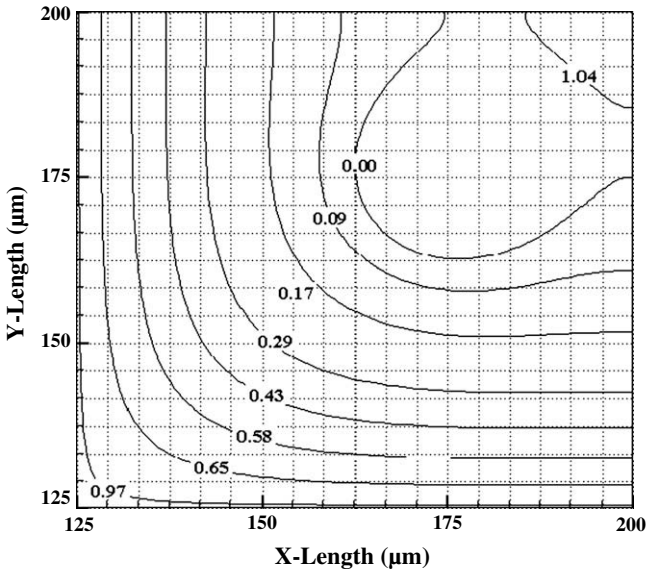

Fig. 4. Thermal distortions contours at dt = 1.96 s, after the simultaneous nucleation of ice within all the four cells, shown in Fig. 1. One of the nucleating cells is centered at (x,y) coordinates of (175,175). The nucleating cell is assumed to be 50 μm in diameter, being cooled at 5 °C/min and ice nucleates within all the cells at −5 °C. Note that at one of the cell centers (175,175) that ΔT = 0 °C. Various isotherms are also shown in the figure.

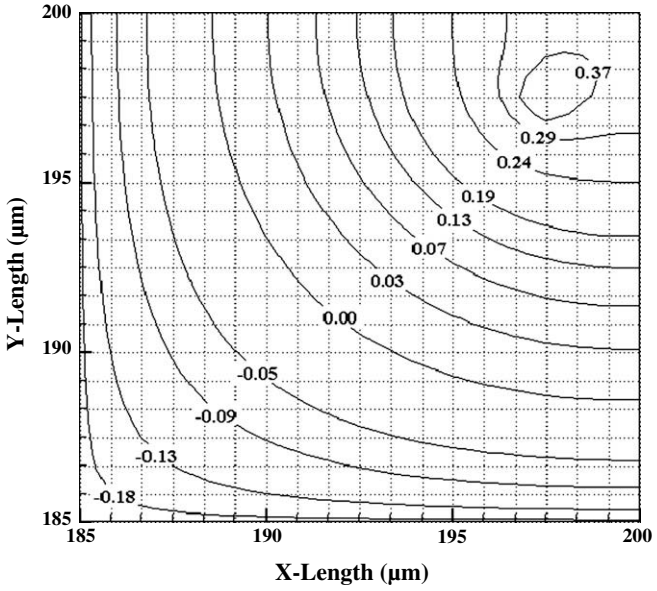

Fig. 5. Immediate ($dt = 0$) thermal distortions due to the simultaneous nucleation of ice within all the four cells, shown in Fig. 1. One of the nucleating cells is centered at (x,y) coordinates of (198,198). The nucleating cell is assumed to be 5 μm in diameter, being cooled at 100 °C/min and ice nucleates within all the cells at −2-0 °C. Note that at one of the cell centers (198,198) that $\Delta T = 0.37$ °C. Various isotherms are also shown in the figure.

cells for Scenario 1 (i.e. a 50 μm cell nucleating at −5 °C while being cooled at 5 °C/min). Note that $dt = 0$ represents the exact instant at which intracellular ice nucleates within the cell (i.e. when $T = T_{nuc}$ at the center of the cell) and the latent heat due to ice nucleating within the super-cooled cell ($Q = \rho_l \cdot \Delta H_f(T_{nuc}) \cdot V$) is released into the computational domain that is still being cooled at a constant and pre-determined cooling rate, in this case at 5 °C/min. The (x,y) coordinates of (175, 175) denote the cell center in both Figs. 3 and 4. Note that the thermal contours in Figs. 3 and 4 show the computed temperature increase within the domain (i.e. the 3rd quadrant of Fig. 1) due to simultaneous ice nucleation inside all the four cells at −5 °C. As shown in Fig. 3, a thermal perturbation of ~1.97 °C is computed at the cell center and the spatial location affected by ice formation within the four cells is exhibited up to a distance of ~25 ± 5 μm from the nucleating cell center.

The symmetric thermal distortion contours when four cells each 5 μm in diameter nucleate at −20 °C and subjected to cooling rate of ~100 °C/min (i.e. Scenario 2) is shown in Fig. 5 ($dt = 0$ s) and Fig. 6 ($dt = 0.04$ s after ice nucleation). The (x,y) coordinates of (198, 198) denote the cell center in both Figs. 5 and 6. Again note that the thermal contours in Figs. 5 and 6 show the computed temperature increase within the domain in the 3rd quadrant of Fig. 1. As expected, in Fig. 5, the thermal distortions are lower than the previous case and the effect of the thermal perturbation is seen locally only up to a distance of ~6 ± 2 μm. It is interesting to observe that at the (x,y) co-ordinates of (200,200) in Fig. 6 (and also in Fig. 4) i.e. a region close to the line of symmetry and consequently to the other nucleating cells, the predicted rise in temperature, ΔT is quite significant. This observation clearly indicates that the model does indeed account for the presence of adjacent cells and the consequent effect in predicted thermal field caused due to cell-cell interactions.

The thermal distortion contours due to nucleation of two cells each 50 μm in diameter, nucleating at −5 °C when cooled at a cooling rate of 5 °C/min is presented in Fig. 7 ($dt = 0$) and Fig. 8 ($dt = 1.27$ s after ice nucleation). The (x,y) coordinates of (175, 150) denote the cell center in both Figs. 7 and 8. The relative thermal distortion at the cell center is ~1.43 °C (Fig. 7) and the thermally effected region is ~70 ± 5 μm from the nucleating cell center (Fig. 8). Similarly, Figs. 9 and 10 show the thermal distortion contours when two cells each 5 μm in diameter nucleate at −20 °C when being cooled at 100 °C/min at $dt = 0$ sec and $dt = 0.03$ s, respectively. The (x,y) coordinates of (195, 150) denote the cell center in both Figs. 9 and 10. The relative thermal distortion in Fig. 9 is ~0.27 °C at the cell center and the thermally effected zone

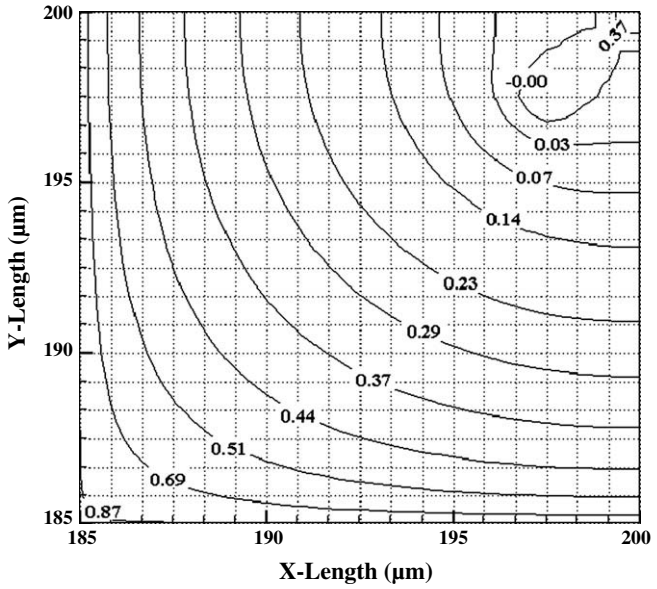

Fig. 6. Thermal distortions contours at $dt = 0.04$ s, after the simultaneous nucleation of ice within all the four cells, shown in Fig. 1. One of the nucleating cells is centered at (x,y) coordinates of (198,198). The nucleating cell is assumed to be 5 μm in diameter, being cooled at 100 °C/min and ice nucleates within this cell at −20 °C. Note that at one of the cell centers (198,198) that $\Delta T = 0$ °C. Various isotherms are also shown in the figure.

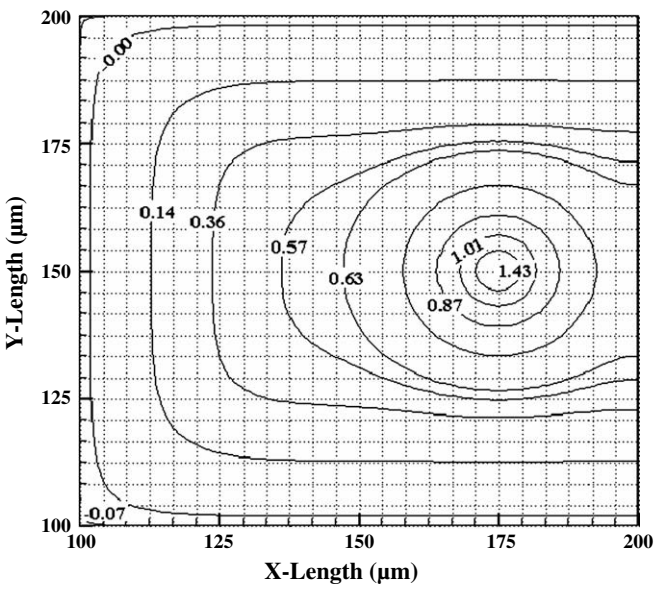

Fig. 7. Immediate ($dt = 0$) thermal distortions due to the simultaneous nucleation of ice within the two cells, shown in Fig. 2. One of the nucleating cells is situated at (x,y) coordinates of (175,150). The nucleating cells are assumed to be 50 μm in diameter, being cooled at 5 °C/min and ice nucleates within each cell at −5 °C. Note that at one of the cell centers (175,150) that $\Delta T = 1.43$ °C. Various isotherms are also shown in the figure.

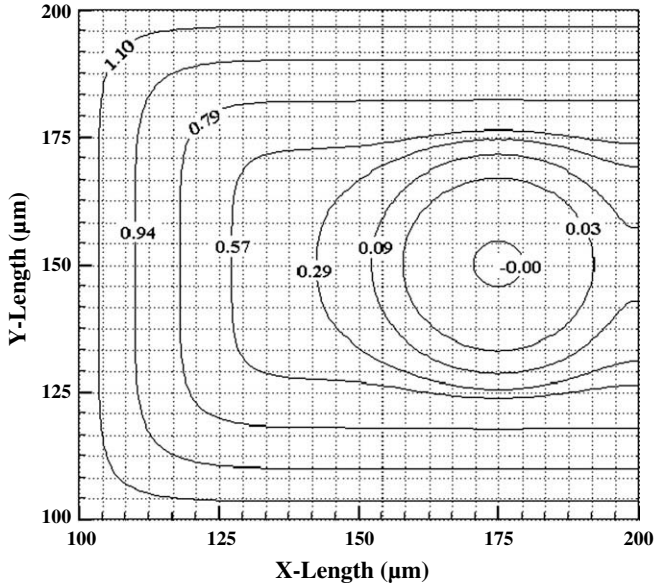

Fig. 8. Thermal distortions contours at dt = 1.27 s, after the simultaneous nucleation of ice within the two cells, shown in Fig. 2. One of the nucleating cells is situated at (x,y) coordinates of (175,150). The nucleating cells are assumed to be 50 μm in diameter, being cooled at 5 °C/min and ice nucleates within each cell at −5 °C. Note that at one of the cell centers (175,150) that ΔT = 0 °C. Various isotherms are also shown in the figure.

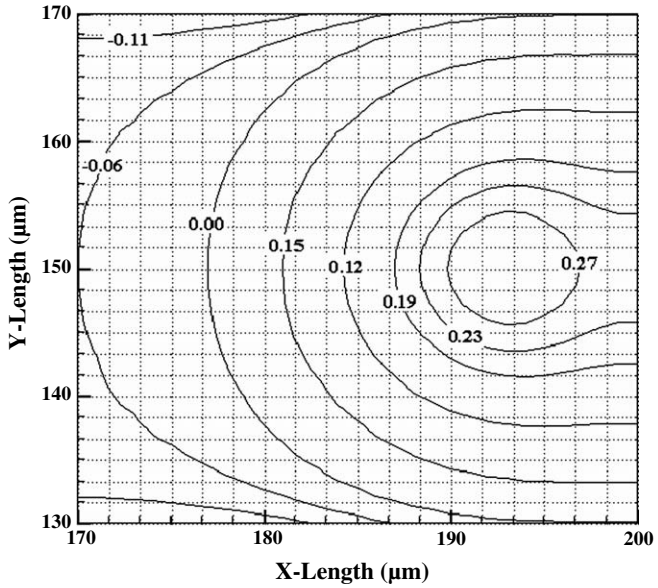

Fig. 9. Immediate (dt = 0) thermal distortions due to the simultaneous nucleation of ice within the two cells, shown in Fig. 2. One of the nucleating cells is situated at (x,y) coordinates of (195,150). The nucleating cells are assumed to be 5 μm in diameter, being cooled at 100 °C/min and ice nucleates within each cell at −20 °C. Note that at one of the cell centers (195,150) that ΔT = 0.27 °C. Various isotherms are also shown in the figure.

is ∼15 ± 5 μm from the nucleating cell center. These and the corresponding results from a single nucleating cell are shown in Table 2 (but in the interest of brevity are not presented graphically).

And finally, to complete our analysis we performed an additional set of extensive experiments assuming a single nucleating cell and the cooling rate varying from 5 °C/min to 100 °C/min with a 2 °C/min increment and for each of these cooling rates we varied the nucleation temperature from −5 °C to −20 °C again with a

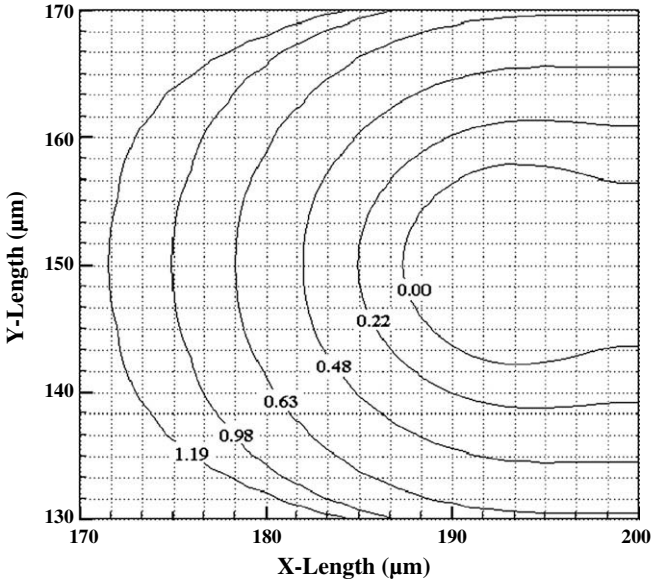

Fig. 10. Thermal distortions contours at dt = 0.03 s, after the simultaneous nucleation of ice within the two cells, shown in Fig. 2. One of the nucleating cells is situated at (x,y) coordinates of (195,150). The nucleating cells are assumed to be 5 μm in diameter, being cooled at 100 °C/min and ice nucleates within each cell at −20 °C. Note that at one of the cell centers (195,150) that ΔT = 0 °C. Various isotherms are also shown in the figure.

−2 °C, increment. We also varied the diameter of the nucleating cell from 5 μm to 50 μm, in increments of 5 μm. Thus, an additional set of ∼4400 simulations were performed to assess the magnitude of ΔT and dt. By utilizing a commercially available log-linear regression analysis statistical software (STATA™, College Station, TX) we found that the results from these extensive set of simulations can be represented as: $\Delta T = \frac{e^{82.85} R^{2.03}}{L^{0.86} B^{0.45} T_{nuc}^{12.51}}$ and $dt = \frac{e^{-5.04} R^{2.97} T_{nuc}^{5.28}}{L^{0.93} B^{0.69}}$.

3.1. Discussion

Recent advances in micro- and nano- fabrication presents an unprecedented opportunity to provide biologists and bioengineers with a set of novel tools that will permit the detailed investigation of previously unquantifiable phenomena. As investigators learn to use and interpret data on the cellular scale, the demand for more capable instruments will continue to increase. As part of this global endeavor we have recently started to design and develop a novel class of instruments based on micro-fabricated thermoelectric sensors and actuators [29,30]. The objective is to micro-fabricate both individual probes and arrays of probes which take advantage of thermoelectric principles to measure (utilizing the Seebeck effect) and modulate (utilizing the Thompson effect) temperature on the cellular level. The devices utilizing the Seebeck effect, i.e., microthermocouples are to be used to measure the nature and extent of intracellular ice formation or ice nucleation within cells embedded in a tissue system. This dynamic information on tissue freezing is currently available and the proposed devices when fabricated, characterized and tested will generate critical data on nucleation phenomena in embedded tissue cells. Since the proposed microthermocouples are based on the Seebeck, effect, which relates to our ability to convert observed temperature changes to electrical voltage, it is clearly necessary to determine *a priori* the local thermal fluctuations during ice nucleation in cells in suspension. This knowledge will be essential to determine the required capability and sensitivity of the proposed device. For example, an examination of the data shown in Table 2, suggests that the micro-thermocouples need to be placed within a spatial distance of ∼10 μm from

Table 2
Computed maximum increase in local temperature due to localized intracellular ice formation in cells (ΔT) and the time (dt) taken for the localized increase in temperature to dampen out to the surrounds under the two scenarios investigated

No. of cells (simultaneously nucleating)	Cooling conditions	Increase in local temperature, ΔT (K)	Time to Dampen local temperature distortion, dt (s)
1	Scenario 1	1.13	1.03
	Scenario 2	0.21	0.01
2	Scenario 1	1.43	1.27
	Scenario 2	0.27	0.03
4	Scenario 1	1.97	1.96
	Scenario 2	0.37	0.04

Scenario 1: Cell diameter = 50 μm; local cooling rate = 5 °C/min and the temperature of ice nucleation within the cells = −5 °C.
Scenario 2: Cell diameter = 5 μm; local cooling rate = 100 °C/min and the temperature of ice nucleation within the cells = −20 °C.

the nucleating cell with an ability to measure local temperature jump of ~0.2 °C and a temporal resolution of ~0.01 secs. Additionally, the simulations presented here are also of value in the development of micro-thermo electric coolers (μTECs), based on the Thompson effect [31,32]. For example, the local thermal fluctuations within the tissue system due to nucleation of ice within the embedded cells can be completely eliminated by cooling the nucleating region with the use of a specifically designed μTEC. Eliminating the local fluctuation within the tissue system during a freezing process might lead to improved post-thaw response, especially when utilized during freezing of highly thermo-sensitive tissues like ovarian tissues.

This study presents a unique combination of the microscale phenomena (IIF) with the macroscale phase change process in biological tissues. The microscale processes are included in the bioheat transfer equation using a source term methodology. However, it should be noted that the model is limited by the lack of tissue intracellular ice formation (IIF) parameters. Briefly, the mechanistic theory of IIF in biological systems is governed by a complex set of equations based on the classical theory of nucleation [33,34], as shown by Toner et al. [35]. Toner's mechanistic model, states that for a thermodynamic system composed of identical biological cells, the probability of intracellular ice formation (PIF) by surface catalyzed nucleation (SCN) or by a volume catalyzed nucleation (VCN) mechanism when the surface catalyzed nucleation mode is suppressed by rapid cooling or in cases where cooling proceeds in the absence of extracellular ice (i.e. the intracellular fluids are supercooled to the volume catalyzed nucleation temperature). The PIF by SCN is governed by, a thermodynamic ice nucleation parameter, Ω_{SCN} and a kinetic ice nucleation parameter, κ_{SCN} and the amount of supercooling. The two nucleation parameters (Ω_{VCN} and κ_{VCN}) for volume catalyzed nucleation are similar to those described above for the surface catalyzed nucleation; however, the form of the overall probability function is slightly different [35–37]. Since the values of the parameters governing IIF in embedded tissue cells are still not available in the literature and since, we were not trying to solve for the exact thermal distortions within the partially frozen domain due to IIF within the cells, we utilized a pre-defined set of nucleation conditions to determine the microscale (local) thermal perturbations. The baseline knowledge gained from this study, albeit being unrealistic to represent an actual tissue system being frozen, is still valuable to rationally design a set of micro-devices such that the PIF in cells embedded in opaque tissue sections can be determined, and consequently the as yet unknown parameters governing the nucleation process.

The present model also neglects the effect of metabolic heat generation and the effect of blood flow on the freezing process (see Eq. (1)). This formulation is clearly less valid for simulating an *in vivo* cryosurgical scenario than an *in vitro* cryopreservation case. In addition, the model presented in this study assumes that the latent heat released by the extracellular solution during the freezing process follows the phase diagram (as stated earlier). One recent study [32] suggests that the latent heat released by the extracellular solution has a cooling rate dependence (i.e. it is both temperature and time dependent). However, we expect, based on our earlier results in the coupled biophysical model [22], that the inclusion of this additional time dependence to the latent heat release to not significantly impact the results presented here. The current model also does not account for the presence of chemicals that are commonly added to biological systems during a freezing process. These chemical denoted as cryoprotective agents (CPAs) have been shown to alleviate the freezing injury and also tend to reduce the latent heat released by the extracellular solution during the freezing process [32]. Thus, the addition of CPAs will most definitely lower the ΔT and dt results obtained in the current study. However, for the purpose of trying to determine *a priori* the specifications for the proposed set of micro-fabricated thermal sensors and actuators, the inclusion of CPAs (and the attendant complex changes to the freezing process), was deemed to be not important. And, contrary to the non-inclusion of metabolic heat generation term discussed earlier, this exclusion of CPAs in our model makes our results more relevant to an *in vivo* cryosurgical process than an *in vitro* cryopreservation protocol. Clearly, future studies are needed.

4. Conclusion

We present a 2-dimensional numerical model that couples the effect of highly localized microscale ice nucleation phenomena to the macroscale freezing process for cells embedded in a tissue system. The results from the numerical model are analyzed to predict the magnitude of perturbations to the local temperature field immediately after ice nucleates within a cell (ΔT) and also the time (dt) it takes for this distortion to dampen out to the local temperature. This knowledge is essential to determine the required sensitivity of a micro-fabricated thermal sensor, currently being developed.

Acknowledgement

This work was supported in part by the department of Mechanical Engineering at LSU and by a grant from the Louisiana Board of Regents to RD (LEQSF 2002-05-RD-A-03). Thanks are due to Tathagata Acharya for help with formatting.

References

[1] I.S. Cooper, Cryogenic surgery a new method of destruction or extirpation of benign or malignant tissues, New Engl. J. Med. 268 (1963) 743–749.
[2] W.W. Bonney, B. Fallon, W.L. Gerber, C.E. Hawtrey, S.A. Loening, A.S. Narayana, C.E. Platz, E.F. Rose, J.C. Sall, J.D. Schmidt, D.A. Culp, Cryosurgery in prostatic cancer: Survival, Urology 19 (1982) 37–43.
[3] M.A. Adson, Resection of liver metastases: When is it worth while? World J. Surg. 11 (1987) 511–520.
[4] W.S. Wong, D.O. Chinn, M. Chinn, J. Chinn, W.L. Tom, W.L. Tom, Cryosurgery as a treatment for prostate carcinoma, Cancer 79 (1997) 963–974.
[5] A. Bernard, B.J. Fuller, Cryopreservation of human oocytes: a review of current problems and perspectives, Human Reproduct. Update 2 (1996) 193–207.
[6] S.H. Day, D.A. Nicoll-Griffith, J.M. Silva, Cryopreservation of rat and human liver slices by rapid freezing, Cryobiology 38 (1999) 154–159.
[7] R.V. Devireddy, B. Fahrig, R.A. Godke, S.P. Leibo, Subzero water transport characteristics of boar spermatozoa confirm observed optimal cooling rates, Mole. Reproduct. Develop. 67 (2004) 446–457.
[8] V. Lunardini, Finite difference methods for freezing and thawing, Heat Transfer in Cold Climates, Van Nostrand Reinhold Co, NY, 1981.
[9] L.J. Hayes, K.R. Diller, Implementation of phase change in numerical models of heat transfer, Int. J. Energy Res. 105 (1983) 431–435.

[10] L.J. Hayes, K.R. Diller, H.J. Chang, H.S. Lee, Prediction of local cooling rates and cell survival during the freezing of a cylindrical specimen, Cryobiology 25 (1988) 67–82.
[11] R.G. Keanini, B. Rubinsky, Optimization of multiprobe cryosurgery, ASME J. Heat Transf. 114 (1992) 796–801.
[12] J.C. Bischof, B. Rubinsky, Microscale heat and mass transfer of vascular and intracellular freezing in the liver, ASME J. Heat Transf. 115 (1993) 1029–1035.
[13] Y. Rabin, A. Shitzer, Numerical solution of the multidimensional freezing problem during cryosurgery, ASME J. Biomech. Eng. 120 (1998) 32–37.
[14] J.Y. Zhang, G.A. Sandison, J.Y. Murthy, L.X. Xu, Numerical simulation for heat transfer in prostate cancer cryosurgery, ASME J. Biomech. Eng. 127 (2005) 279–294.
[15] R.M. Love, The freezing of animal tissue, in: H.T. Meryman (Ed.), Cryobiology, Academic Press, London, 1966 (Chapter 7).
[16] B. Rubinsky, C.Y. Lee, J. Bastacky, T.L. Hayes, The mechanism of freezing process in biological tissue, Cryo-letters (1987) 370–381.
[17] J.C. Bischof, K. Christov, B. Rubinsky, A morphological study of cooling rate response in normal and neoplastic human liver tissue: Cryosurgical implications, Cryobiology 30 (1993) 482–492.
[18] P.V. Pazhayannur, J.C. Bischof, Measurement and simulation of water transport during freezing in mammalian liver tissue, ASME J. Biomech. Eng. 119 (1997) 269–277.
[19] R.V. Devireddy, J.C. Bischof, Measurement of water transport during freezing in mammalian liver tissue-Part II: The use of differential scanning calorimetry, ASME J. Biomech. Eng. 120 (1998) 559–569.
[20] R.V. Devireddy, D.J. Smith, J.C. Bischof, Mass transfer during freezing in rat prostate tumor tissue, Am. Inst. Chem. Eng. J. 45 (1999) 639–654.
[21] B. Rubinsky, D.E. Pegg, A mathematical model for the freezing process in biological tissue, Proc. Roy Soc. Lond. B 234 (1988) 343–358.
[22] R.V. Devireddy, D.J. Smith, J.C. Bischof, Effect of microscale mass transport and phase change on numerical prediction of freezing in biological tissues, ASME J. Heat Transf. 124 (2002) 365–374.
[23] V. Alexiades, A.D. Solomon, Mathematical Modeling of Melting and Freezing Processes, Hemisphere Publishing Corporation, Washington, 1993.
[24] M.N. Ozisik, Finite Difference Methods in Heat Transfer, CRC Press, Boca Raton, FL, 1994.
[25] R.V. Devireddy, Quantification of freezing processes in biological systems, Ph. D. Thesis, University of Minnesota, Minneapolis, MN, 1999.
[26] S.V. Patankar, Numerical Heat Transfer and Fluid Flow, Hemisphere Publishing Services Limited, New York, 1980.
[27] H.S. Carslaw, J.C. Jaeger, Conduction of Heat in Solids, second ed., Oxford Science Publications, 1959.
[28] F.P. Incropera, D.P. DeWitt, Introduction to Heat Transfer, third ed., John Wiley and Sons, 1996.
[29] A. Cygan, A. Prabhakar, E.J. Podlaha-Murphy, M.C. Murphy, R.V. Devireddy, Fabrication of micro scale arrays of thermoelectric sensors and actuators for cryobiological applications, American Society of Mechanical Engineers, International Mechanical Engineering Congress and Exposition, CD-ROM Publication, Anaheim, CA, 2004.
[30] A. Cygan, A. Kardak, D. Patterson, E.J. Podlaha-Murphy, R.V. Devireddy, M.C. Murphy, Modeling and fabrication of a microthermocouple array, American Society of Mechanical Engineers, International Mechanical Engineering Congress and Exposition, Winter Annual Meeting, CD-ROM Publication, ASME, New York, NY, 2006.
[31] A. Prabhakar, E.J. Podlaha-Murphy, M.C. Murphy, R.V. Devireddy, Electrodeposition characteristics of bismuth–telluride films, Nanoscale Materials Science in Biology and Medicine, in: C.T. Laurencin, E.A. Botchwey (Eds.), Material Research Society Symposium, 845, Paper number AA5.25, Warrendale, PA, 2004.
[32] A. Prabhakar, M.C. Murphy, R.V. Devireddy, Modeling of bio-thermo-electric micro-cooler, Open Biotechnol. J. 1 (2007) 1–8.
[33] D. Turnbull, J.C. Fisher, Rate of nucleation in condensed systems, J. Chem. Phys. 17 (1949) 71–73.
[34] D. Turnbull, B. Vonegut, Nucleation catalysis, Indust. Eng. Chem. Res. 44 (1951) 1292–1298.
[35] M. Toner, E.G. Cravalho, M. Karel, Thermodynamics and kinetics of intracellular ice formation during freezing of biological cells, J. Appl. Phys. 67 (1990) 1582–1593.
[36] M. Toner, R.G. Tompkins, E.G. Cravalho, M.L. Yarmush, Transport phenomena during freezing of isolated hepatocytes, Am. Inst. Chem. Eng. J. 38 (1992) 1512–1522.
[37] M. Toner, Nucleation of ice crystals in biological cells, in: P.L. Stenponkus (Ed.), Advances in Low Temperature Biology, JAI Press, London, 1993 (Chapter 1).